Available online at www.sciencedirect.com
SCIENCE DIRECT
Polymer 46 (2005) 6437–6446
polymer
www.elsevier.com/locate/polymer

Polypropylene/polyamide 6/polyethylene-octene elastomer blends. Part 3. Mechanisms of volume dilatation during plastic deformation under uniaxial tension

Shu-Lin Bai[a], Christian G'Sell[b,*], Jean-Marie Hiver[c], Cyrille Mathieu[c]

[a]*Department of Mechanics and Engineering Science, Peking University, 100871 Beijing, People's Republic of China*
[b]*Laboratoire de Physique des Matériaux, Ecole des Mines de Nancy, Parc de Saurupt, 54042 Nancy cedex, France*
[c]*Laboratoire d'Etude des Matériaux, Cerdato, Arkema, 27470 Serquigny, France*

Received 16 December 2004; received in revised form 9 March 2005; accepted 11 March 2005

Abstract

It has been shown in a previous paper in this series that important dilatation is produced by plastic deformation under tension of neat PP and PP/PA6/POE blends, for which the POE to PA6 concentration ratio equals 1/2. In this work, the detailed mechanisms of this volume change are investigated from electron micrographs (SEM and TEM) obtained in the deformed state. At low alloy content, it is thus observed that dilatation results from decohesion of the PA6 particles from the PP matrix. As the amount of PA6 and POE increases, voids are nucleated preferentially in the thicker POE interphase making a shell around the PA6 particles, and secondarily in isolated POE particles. Unexpectedly, it has been found that the overall volume dilatation decreases with total alloying content. This is interpreted by: (i) the increasing contribution of PA6 that intrinsically deforms with less cavitation than PP, (ii) the post-cavitation rubber-like stretching of POE particles and, (iii) the early formation of a percolating network of shear bands from the diffuse array of voids formed after the yield point. These mechanisms explain the gradual increase of the resistance to impact of the PP/PA6/POE as their alloying content is increased.

Keywords: Polymer blends; Volume dilatation; Electron microscopy

1. Introduction

Development of cavitation is now recognized as the leading dissipation process during the deformation of polymer blends, which largely controls their resistance to impact [1,2]. As such, it has been shown [3] that cavitation relieves the hydrostatic tension in the matrix, increases deviatoric stresses and promotes shear deformation. The contribution of cavitation proved to be essential to ensure enough plasticity in zones of highly triaxial stress field, notably at crack tips. Furthermore many authors [4] have stated that dispersed rubber-like particles constitute preferential sites of cavitation due to the contrast of elastic modulus with the matrix. Such particles can be plain elastomer droplets, but core-shell nodules (in which the elastomer occupies a thin envelope only) are even more efficient, since the shell undergoes cavitation while the core ensures sufficient rigidity.

In two previous papers of this series [5,6], we have investigated the initial microstructures and mechanical properties of blends composed of polypropylene, polyamide 6 and polyethylene-octene elastomer (PP/PA6/POE for short). Particular attention has been paid to the large volume dilatation measured during tensile deformation by means of a specially developed multiaxial extensometer. The specific interest of this method was that it provides macroscopic information to follow quantitatively the development of cavitation in the course of a tensile test operated at constant true strain rate. However, it is now essential to determine which processes actually control void nucleation and growth in the materials. Also, we aim understanding how the microstructures of the different blends behave specifically with regards to the dilatation process.

* Corresponding author. Tel.: +33 3 83 58 41 54; fax: +33 3 83 57 97 94.
E-mail addresses: slbai@pku.edu.cn (S.-L. Bai), gsell@mines.u-nancy.fr (C. G'Sell).

0032-3861/$ - see front matter © 2005 Elsevier Ltd. All rights reserved.
doi:10.1016/j.polymer.2005.03.111

Other researchers have already contributed to the characterization of deformation damage mechanisms in polymer blends based on polypropylene and polyamides. Wong and Mai [7,8], for a blend system containing a polyamide different to ours (PP/PA66/SEBS) showed evidence of cavitation in the plastic zone ahead of a crack under bending. They noted the preferential formation of voids in the rubber interphase (SEBS) between the matrix and the particles. Also González-Montiel et al. [9–11], working with the PP/PA6/EPR system, consistently found that cavitation is activated in the rubber interphase and in the dispersed rubber particles as well. Unfortunately, the results of the latter authors do not definitively resolve our problem because: (i) the compositions of the samples correspond to the PA6-rich side of the system only and, (ii) the local true strain at which the micrographs were obtained is not precisely indicated, only the nominal strain of the sample being given.

Considering the fundamental importance to model the cavitation processes in PP-rich blends containing diverse kinds of immiscible particles (core-shell PA6/POE and isolated POE), we propose in this paper to analyze the deformed microstructure in specimens stretched under uniaxial tension in well-defined conditions, at constant true strain rate. The observed samples were precisely cut out of the representative volume element (RVE) in which local true strain was measured. The material was properly etched or stained with relevant chemicals to enhance the contrast of the phases. Subsequently, scanning electron microscopy (SEM) and transmission electron microscopy (TEM) were complementarily used in order to characterize the processes at different scale. As such, valuable microscopic information is expected in addition to the quantitative macroscopic data presented in the first papers of the series.

2. Experimental techniques

The neat polypropylene (PP) and the four PP/PA6/POE blends investigated here are the same as in both previous papers. Their processing conditions were explained in details in reference [5]. Their compositions are just recalled in Table 1. One notes that the PP is the major polymer and that the weight fraction of the POE is systematically half that of the PA6. The role of the POE is to act as a compatibilizing agent between PP and PA6; in order to enhance this function, it was grafted with maleic anhydride prior mixing with PP and PA6.

Table 1
Compositions of the blends

Blend	PP (wt%)	PA6 (wt%)	POE (wt%)
PP	100	–	–
BD13	85	10	5
BD14	70	20	10
BD15	55	30	15
BD16	40	40	20

The tensile tests were performed with the VidéoTraction© system (Apollor, Vandoeuvre, France) that gives access in real time to the true axial stress vs. true axial strain curve, $\sigma_{33}(\varepsilon_{33})$, together with the quantitative evolution of the volume strain $\varepsilon_v(\varepsilon_{33})$. The multiaxial video extensometer specially developed for measuring the volume changes in situ in the RVE was detailed elsewhere [6,12]. The tests were terminated by halting the strain-rate and unloading rapidly the samples for a prescribed value of true strain in the RVE.

The first technique used to reveal the internal microstructure was the SEM observation of cryo-fractured surfaces. This protocol preserves the in situ features of the sample, since no further plastic mechanisms is supposed to occur at the temperature of boiling nitrogen. By contrast to usual procedures, where cryo-fractured plane is perpendicular to the axis of the tensile specimens, we chose here to expose a surface parallel to the tensile axis (Fig. 1).

As such, we expect characterizing the damage process in relationship to the local degree of orientation of the microstructure. The cutting plane passes straight along the core line of the sample. Since, all specimens exhibit early plastic instability, the narrowest part of the neck corresponds to the RVE, where the local true strain was recorded by the VidéoTraction© system when the test was halted. We will systematically indicate this value with the micrographs. After cryo-fracture, two different procedures were applied: (i) for some samples, the exposed surface was observed directly in the SEM without any other treatment than the necessary gold coating and, (ii) for others, the surface was slightly polished and subsequently etched with a solution of 32.9% H_3PO_4/65.8% H_2SO_4/1.3% $KMnO_4$. This mixture is known [13] to attack preferentially the amorphous phase of PP and provides more relief on the lamellar structure. In all cases, the microscope utilized was a Jeol JSM-820.

The deformed samples were also observed under TEM. For this purpose, ultra thin sections, less than 1 μm thick, were cut from the samples with an ultra cryo-microtome (Reichert Ultracut E) at a temperature of about −100 °C.

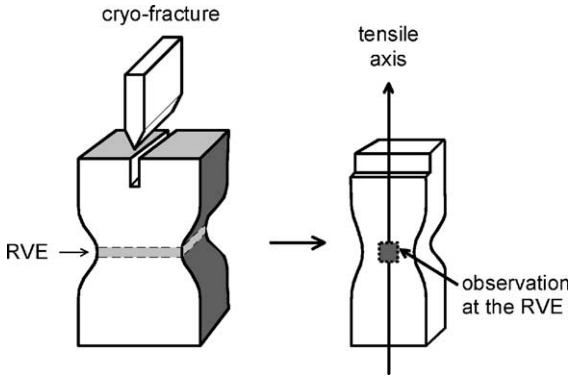

Fig. 1. Methods to prepare the cryo-fractured surfaces for SEM observation.

Similarly to the cryo-fracture surfaces, the microtomed sections were cut in the core region of the specimens parallel to the tensile axis, at the level of the RVE. Consequently, the features that are observed herein also correspond to the true strain recorded at the end of the tensile test. The sections were subsequently stained with vapors of RuO_4 for about 2.5 h. This staining agent was preferred to OsO_4 since, it reacts more likely with the POE elastomer and provides a good contrast to this phase that would not be distinctly observed otherwise [14,15]. Finally the samples were observed in the TEM (Zeiss EM 902) equipped with a tungsten filament and adjusted for an accelerating voltage of 80 kV.

3. Experimental results

3.1. Macroscopic dilatation

In the second paper of this series [6], the curves of volume dilatation vs. axial strain were determined and discussed in details for the neat PP and the four blends. Also for comparison, the behavior of a reference neat PA6 was presented. Here, in order to facilitate the understanding of the dilatation mechanisms, these curves are shown again in Fig. 2. It is seen that depending on the materials, the tests were stopped at different strains varying from 1.2 to 1.6. The tendency for cavitation, measured by the volume strain ($\varepsilon_v = \ln(V/V_0)$, where V represents the volume of the RVE) is evidently dependent on the alloy content. The first striking feature of this graph is the fairly high dilatation of the neat PP ($\varepsilon_v = 0.47$ for $\varepsilon_{33} = 1.4$). This was observed earlier by Lazzeri et al. [16], using a less sophisticated strain-gauge technique, and interpreted in terms of a microvoiding process. The second one is the general decrease of the cavitation tendency when the overall alloying content is increased. Except for the BD13 alloy that dilates a little bit more than neat PP, one sees that the $\varepsilon_v(\varepsilon_{33})$ curves are well below for the blends than for PP. For the highest alloying content (BD 16), the volume strain is only half that of PP. Also, it is noted that the neat PA6 exhibits very conservative deformation, since volume strain hardly goes above 0.1 when axial strain reaches 1.0.

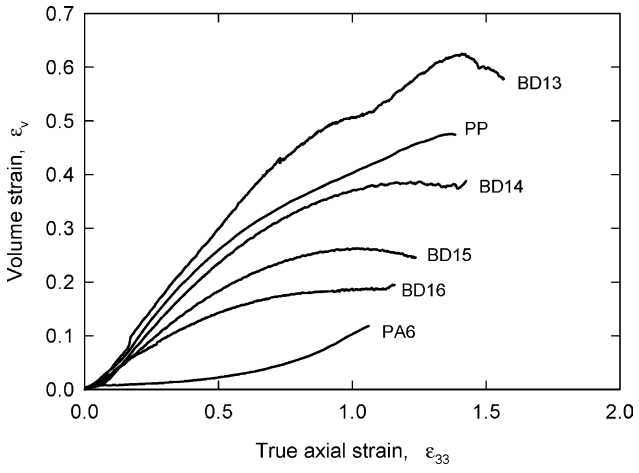

Fig. 2. Volume strain vs. true axial strain.

3.2. SEM characterization of neat PP

In the case of a semi-crystalline polymer like PP, the microstructural features are likely to appear at the scale of the spherulites (typically 5–100 μm in diameter), or even closer at the scale of the long period of the lamellar stacks (10–100 nm). In order to accede to the latter details, it was shown previously [17] that etching of the polished surface with oxidizing acids engraves the amorphous interstices and lets the crystalline morphology appear: lamellae, or at least stacks of lamellae, become visible.

Fig. 3(a) shows a micrograph of neat PP obtained in the undeformed state. It confirms the spherulitic nature of the

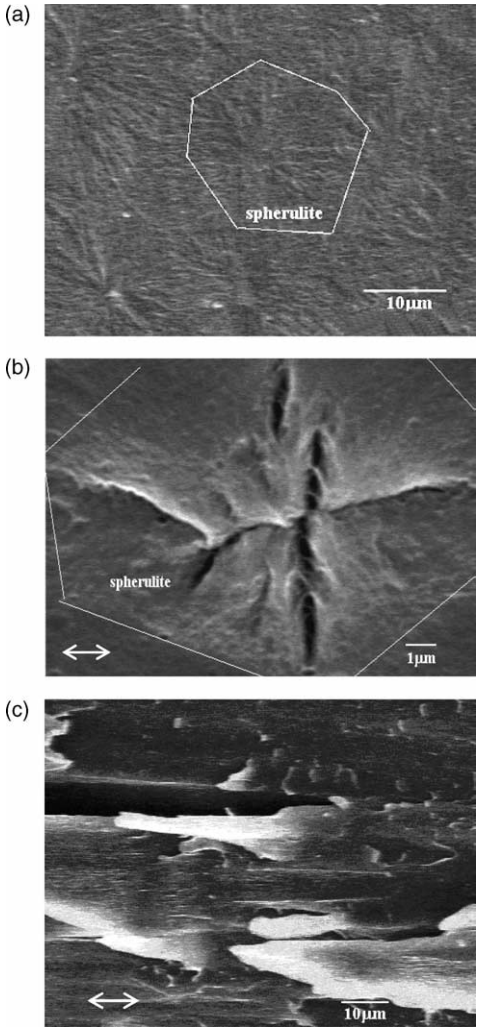

Fig. 3. SEM observation of neat PP etched with an acid solution, (a) evidence of spherulitic morphology at $\varepsilon_{33} \approx 0$, (b) microcracks in the core of a spherulite at $\varepsilon_{33} \approx 1.2$, (c) elongated crack observed at low magnification at $\varepsilon_{33} \approx 1.2$ (arrows indicates the tensile direction).

morphology in this PP whose crystalline fraction (51 wt% measured by DSC) is totally composed of monoclinic α modification. One spherulite in the center of the micrograph is outlined with a very regular polyhedral shape and an average diameter of about 20 μm. Although the individual lamellae are hardly resolved at that scale, the radial growth direction appears clearly.

Fig. 3(b) was obtained with the same protocol, but after a tensile test interrupted at a strain $\varepsilon_{33} \approx 1.2$, that corresponds to a stretch ratio, $\lambda = \exp(\varepsilon_{33})$, of about 3.3. It shows essentially one spherulite elongated along the tensile direction (horizontal). The major feature visible is a network of microcracks within the spherulite. The microcracks are oriented along various radial directions of crystal lamellae, not only in the direction perpendicular to the tensile axis. Also, it seems that they stopped growing when approaching the boundary with an adjacent spherulite. No interspherulitic decohesion was observed in this polymer. The above results are in good agreement with those of Aboulfaraj et al. [18] who found that, under tension, the crazes in the α-PP appear preferentially at the centre of the spherulites, grow parallel to radial directions and eventually reorient their propagation direction perpendicular to the tensile axis. Others have shown [19] that the early stage of spherulite damage corresponds to the fragmentation of semi-crystalline stacks after shear and bending under the constraint of tie molecules.

Fig. 3(c) corresponds to the same strain but at a much lesser magnification. Now it is no longer possible to resolve any crystalline morphology. In place, one observes cracks highly elongated in the tensile direction. The size of the cracks is of the order of 10 μm in width and more than 100 μm in length. It seems that these defects represent the ultimate evolution of the spherulite microcracks under the effect of large plastic deformation. Consequently, the highly stretched polymer can be regarded as an anisotropic porous structure composed of ultra-oriented fibrils separating such oriented cracks. The volume strain measured with the VidéoTraction© system at $\varepsilon_{33} \approx 1.2$ being equal to $\varepsilon_v \approx 0.42$, the void fraction in RVE of the stretched specimen is thus: $(V - V_s)/V_s = \exp(\varepsilon_v) \approx 52\%$.

3.3. SEM characterization of polished and etched blends

For the BD13 blend (smaller alloying content), the SEM micrograph of Fig. 4(a) was obtained at a strain $\varepsilon_{33} \approx 1.6$ after polishing and etching. Like in highly deformed PP one sees a high density of parallel cracks oriented along the tensile direction. No PA6 nodule is visible here because these particles are systematically removed by the acid etching as shown in a previous paper [5].

Corresponding observation for the BD14 blend, deformed at $\varepsilon_{33} \approx 1.4$ is shown in Fig. 4(b). Similar unidirectional cracks are seen along the loading direction. However, now the cracks are both lesser and smaller.

For the BD15 blend after stretching up to $\varepsilon_{33} \approx 1.25$ (Fig. 4(c)) the decrease of crack number and size is continued. In particular the length of the cracks is much smaller and also they seem less open.

Finally in the BD16 blend deformed up to $\varepsilon_{33} \approx 1.2$ (Fig. 4(d)) the morphology indicates not only that the evolution with alloying content continues towards less

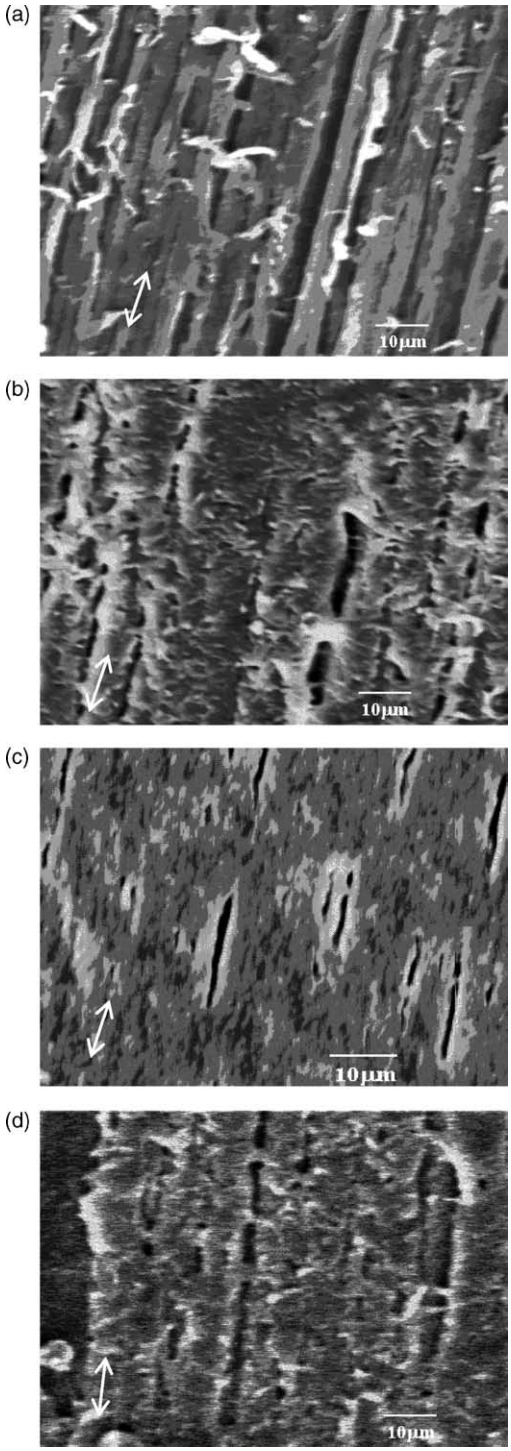

Fig. 4. SEM micrographs of deformed blends after cryo-fracture, polishing and etching, (a) BD13 at $\varepsilon_{33} \approx 1.6$; (b) BD14 at $\varepsilon_{33} \approx 1.4$; (c) BD15 at $\varepsilon_{33} \approx 1.25$; (d) BD16 at $\varepsilon_{33} \approx 1.2$.

severe damage, but also it is evident that the deformation mechanisms themselves have qualitatively changed. The rather regular ligaments observed in previous specimens are now replaced by a profusion of shear debris looking like disordered polymer ribbons. This is a typical sign that cavitation process (still active) is now in competition with extensive plastic deformation mechanisms.

Several remarks should be done about the above results. Although it is probable that the acid has amplified somehow the size of the crack by dissolving some amorphous zones of the material, especially at thin fibrils, this effect is moderate, as we will check it below in non-etched samples. Also it is ascertained that the acid has systematically dissolved the PA6 nodules. Despite these artifacts, observation of etched surfaces from within the deformed blends provides a relevant view of crack configuration as a function of blend composition. As such, the most significant properties established at that point are: (i) the development of highly elongated voids from initial crazes in the stretched samples, (ii) the fibrillated morphology of the polymer ligaments between the longitudinal voids and, (iii) the growing importance of plastic deformation processes with respect to the damage mechanisms as the alloying content of the blends is increased.

3.4. SEM characterization of simply cryo-fractured blends

In this section, we will examine SEM micrographs obtained on surfaces exposed by cryo-fracture without further treatment (except again the gold coating stage). The true strains at which the tests were halted for these specimens were systematically the same as in Section 3.3. Since, the aim of this observation was to identify the craze initiation mechanisms, the images under consideration were preferentially chosen at a magnification higher than the ones above.

The typical micrograph in Fig. 5(a) was obtained with a BD13 specimen. Again long voids oriented along the tensile axis are the most characteristic features. It is interesting to note that these channels are empty, no fibrils being visible in the interior. This observation corroborates what was found in the etched samples and proves that the oxidizing acids did not modify excessively the general morphology. Now the dispersed PA6 particles are visible. They appear like isolated beads, with a size of the order of 1 μm, resting within the elongated voids, with apparently little connectivity with the neighboring material. Although the overall strain is very large, it is interesting to remark that the ellipticity of the PA6 nodules is small, which means that decohesion at their interface with the PP should have occurred early during the tensile test. The tiny droplets that are seen inside the PA6 nodules, like in 'salami' morphology, have been ascribed to as PP inclusions. They do not play a significant role in the deformation mechanisms. As for the POE phase it presumably constitutes the long filaments joining PA6 particles and

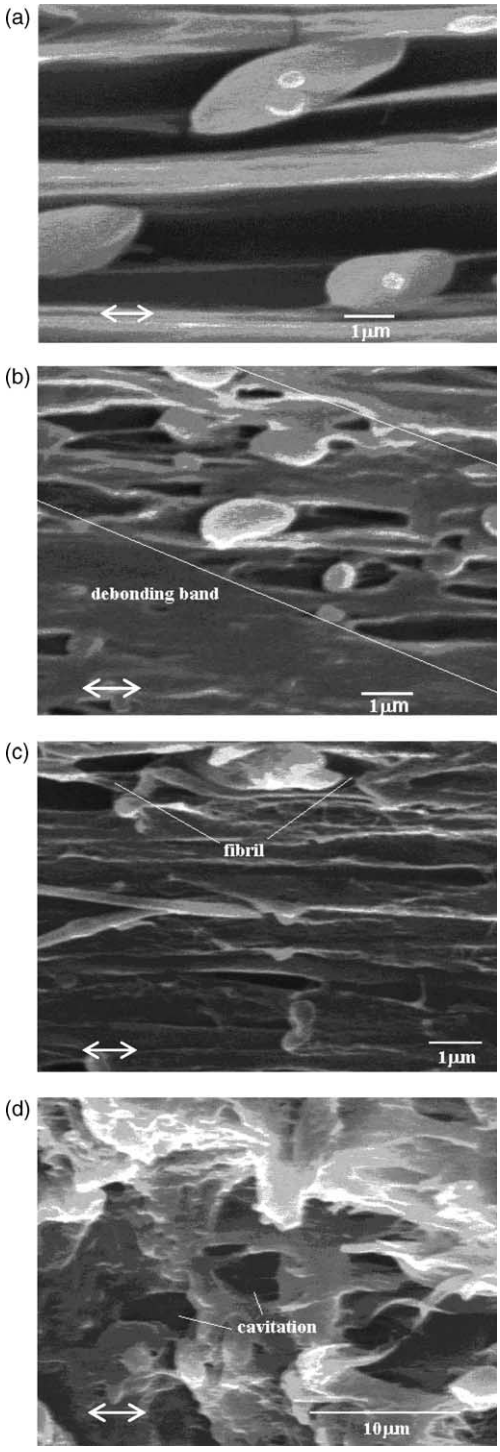

Fig. 5. SEM micrographs of deformed blends after simple cryo-fracture, (a) BD13; (b) BD14; (c) BD15; (d) BD16 (same strains as in Fig. 4).

the matrix. Since, it was shown in a previous paper [5] that at low alloying content the POE shell surrounding the PA6 particles is very thin (if any), it is probable that decohesion occurs in the polar region of the particles, forming arc-cracks at the weaker POE/PP interface. Further growth of these cracks leads to total detachment of the particle. At large strain, the voids resulting from this decohesion are

transformed into highly elongated cracks that presumably coalesce one another giving rise to those continuous 'empty channels'.

In the BD14 blend (Fig. 5(b)) deformation damage is less active than in BD13. At that scale, it appears that the elongated cracks are no longer continuous. Since the POE interphase is now thicker, damage results both from decohesion at the interface POE/PP matrix, and also in some cases from the cavitation inside the shell (following a mechanism described in the literature [3]). Additionally some decohesion is observed at smaller particles, presumably isolated POE droplets dispersed in the PP matrix. For the latter, the voids do not develop so much and most particles remains attached to the matrix. If we consider now the distribution of defects, it is seen that voids are preferentially localized in certain places, where the particles (PA6 or POE) are close to each other. The micrograph shows a row of voids forming a kind of 'decohesion band' that resembles to the typical configurations presented in the literature [20].

The evolution identified above continues in the case of the BD15 blend shown in Fig. 5(c). In the upper part of the micrograph one sees a big PA6 particle with one void at each pole. It seems that some fibrils are present herein that probably result from the stretching of pieces of POE partially detached from the thick interphase. Now the cracks represent only a limited fraction of the surface and their length is smaller. As for the PP matrix, it presents more evidence of shear debris appearing as white 'waves' at the border of some oriented voids.

Finally in the BD16 blend, the micrograph in Fig. 5(d) shows a variety of configurations representative of cavitation and shear mechanisms, the deformation being evidently more conservative than in the other blends. Cracks remain numerous (with a diameter of about 50 μm) but now their ellipticity is much lesser. Between these defects, one notes a distribution of polymer 'ribbons' that presumably result from the shear processes that play the major role in the stretch deformation. The holes surrounded by such ribbons, which look like 'bird nests', can thus be considered as the most specific defects observed in this highly alloyed blend. To some extent, they corresponds to configurations observed previously by Gonzáles-Montiel [11] presented as fibril bridging the space between nylon 6 particle and PP matrix for a 50% PP/50% PA6 blend compatibilized with SEBS or EPR.

3.5. TEM characterization of stained sections of blends

The TEM observation after staining with RuO_4 provides us with high-definition view of the microscopic mechanisms and reveals the specific role of the POE phase.

In the BD13 blend, shown in Fig. 6(a), three phenomena are visible: (i) interfacial debonding at the poles of PA6 particles, (ii) high elongation of hyperelastic POE particles, and (iii) cavitation in dispersed POE droplets. On the overall

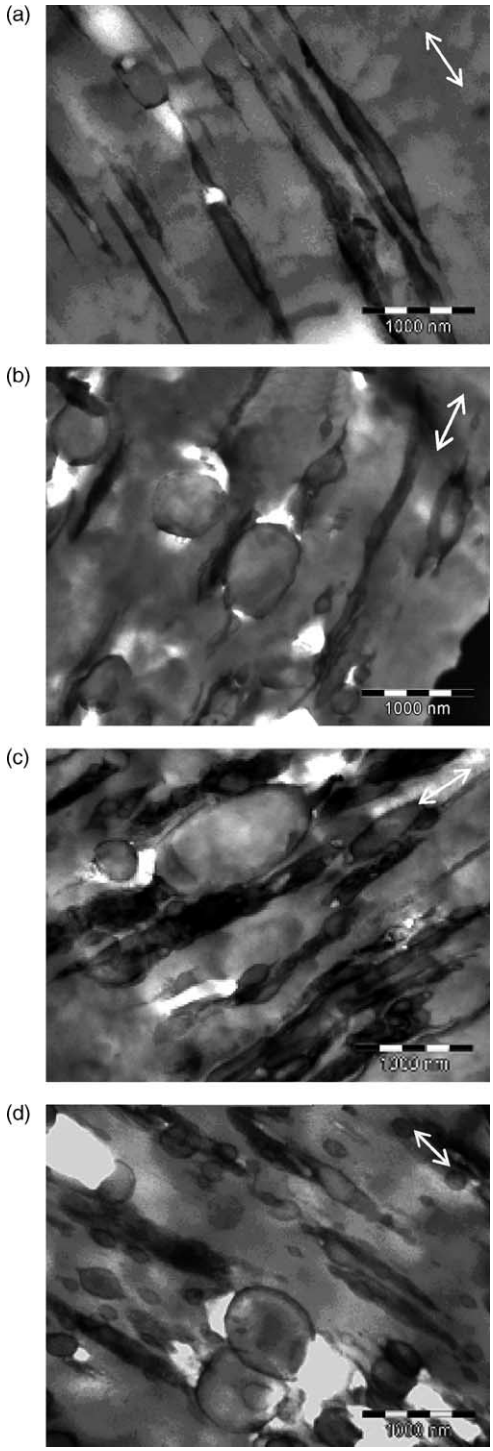

Fig. 6. TEM micrographs of deformed blends after straining with RuO_4 vapor: (a) BD13; (b) BD14; (c) BD15; (d) BD16 (same strains as in Figs. 4 and 5).

since, the size and number of POE particles are smaller than that of PA6 particles the former mechanism is more frequently observed and seems to have a leading influence on the overall volume strain.

For BD14, Fig. 6(b) interfacial debonding represents the main damage factor like in BD13. It occurs preferentially

around largest PA6 particles. Some smaller PA6 particles seem intact, even though their POE shell has been strongly stretched in the loading direction. Again the volume increase comes preferentially from the debonding of PA6 particles. However, it is interesting to note that cavitation inside the PA6 phase is never observed.

For BD15, with an alloying content of 45 wt%, Fig. 6(c) the cavitation at the poles of PA6 particles seems to result more from the cavitation of the POE interphase than from a simple interfacial debonding (although it is not always simple to make the difference). Also the cavitation in dispersed POE droplets is very active. Furthermore, in some micrographs, a new type of 'salami' structure is present: large POE nodule containing small PA6 inclusions. Under uniaxial tension, the POE of these 'salami' structures deforms easily, while the PA6 particles inside seem unaffected.

At last for BD16 (Fig. 6(d)), in which PP is in minority, cavitation occurs more likely in POE interphase at the poles of large PA6 particles and in large isolated POE particles (that are more numerous in this blend). However, conservative deformation mechanisms become predominant and are commonly identified: (i) at smaller POE droplets, (ii) at 'salami' structures and, (iii) in the PP matrix.

4. Discussion

The above morphological characterization helps us to understand the influence of composition on the dilatation of the materials under uniaxial tension.

For neat PP, the crazing mechanisms have been the object of many previous papers [18,19,21]. It was shown that crazes resulting from early fragmentation of the crystalline stacks propagate in the amorphous phase between the lamellae along the radial directions as shown in Fig. 7. At higher strain the cracks are rotated and become nearly parallel to the tensile direction. It is remarkable that such damage phenomena were early discovered, they did not convince previous authors of the importance of volume strain in PP. Consequently, in the mechanical engineering community, finite element codes applied to the prediction of large deformation in PP parts (e.g. for the optimization of shock absorbers) make implicitly the assumption that the plastic response is isochoric ($\varepsilon_v = 0$) as soon as the yield point is passed. As such, the quantitative dilatation measurements published in the second paper of this series [6], related to the microscopic observation presented here, establish the statement that the important volume increase undergone by neat PP under tension is the direct consequence of the development of crazes and the elongation of voids in the spherulitic structure.

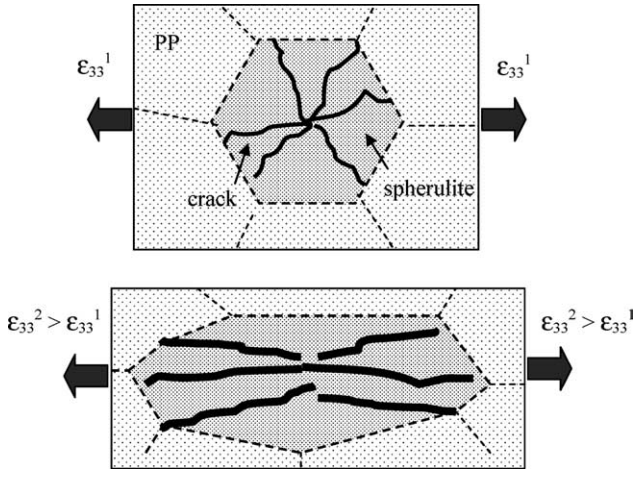

Fig. 7. Schematic evolution of cracks in a PP spherulite for moderate and large applied strain in uniaxial tension.

In the case of the ternary blends, the difficulty for modeling the behavior comes essentially from the multiplicity of phase configurations. In the case of PP/PA6/POE blends, the three components are not chemically compatible but the maleic anhydride grafted on POE elastomer chains provides it with a certain affinity for the PA6. Consequently, most of the POE migrates spontaneously during the mixing sequence towards the interface of the PA6 nodules, where it forms a peripheral interphase like in a 'core-shell' particle with a stiff interior (PA6) and a thin rubbery envelope (POE). However, at high alloying content, the thickness of the interphase becomes too large and the compatibilizer in excess precipitates into isolated particles. As we saw in different micrographs, more complex configurations are found, notably 'salami'-type nodules with PP droplets inside the core of PA6–POE particles or with PA6 droplets within a big POE particle. Also in the case of the blend with the highest alloying content, special 'clusters' of agglomerated PA6 and POE particles were identified. These different configurations are summarized schematically in Fig. 8.

When the blends are subjected to tensile testing, a certain fraction of the overall strain is accommodated by conservative deformation of the material. In the PP matrix, deformation results from the combination of amorphous phase hyperelasticity and crystal plasticity, as discussed earlier [22]. The PA6 phase is also capable to deform plastically but its flow stress in the plastic stage is much higher than that of PP [6]. Consequently in the PP/PA6 blends the isolated PA6 particles exhibit less deformation than the PP matrix, leading to interfacial stress concentrations. By contrast the isolated POE nodules deform easily due to the rubber-like properties of the compatibilizer. It is thus logical to observe highly elongated POE particles in the stretched blend samples. At last for the POE–PA6 'salami' nodules, they deform easily but the PA6 inclusions inside remain nearly undeformed. The deformed configurations are shown in Fig. 9.

As revealed by the ε_v vs. ε_{33} curves obtained by means of the VidéoTraction© system (Fig. 2) cavitation plays an important role in the deformation of the blends investigated

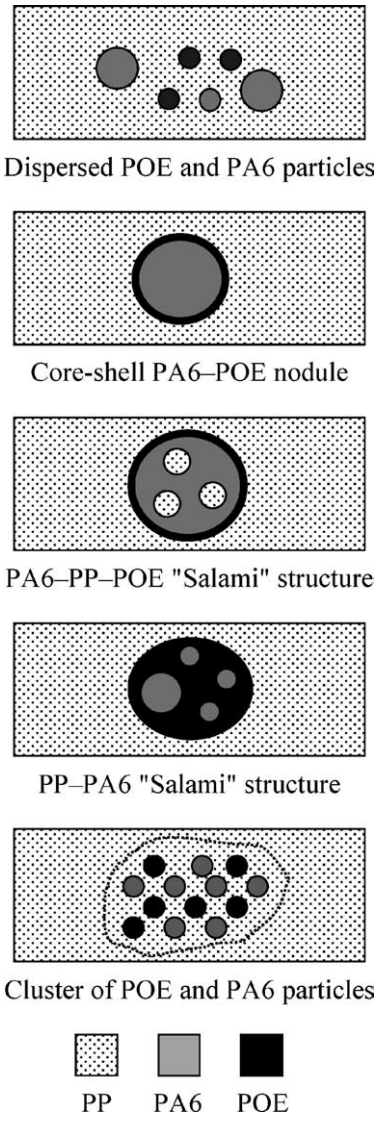

Fig. 8. Schematic representation of the different particles in the PP/PA6/POE blends.

here. The micrographs shown above revealed the various mechanisms creating voids for the different morphological configurations. The major ones (non-exhaustively) are shown in Fig. 10. One class of damage mechanism corresponds to interfacial debonding. Due to the contrast in the mechanical properties of adjacent materials, the induced stresses break the weak adhesion leading to arc-crack preferentially developing at the poles. Interfacial debonding is principally active for isolated PA6 particles, less for isolated POE particles. As for the PA6–POE core-shell nodules, decohesion seems to affect primarily the POE/PP interface. Although decohesion is the most active damage mechanism for blends with low alloying content (BD13 and BD14) another process appears as the size of the POE domains increases. It has been shown by many authors [3,4] that a rubber-like inclusion embedded in a deformed matrix undergoes high hydrostatic stress and eventually

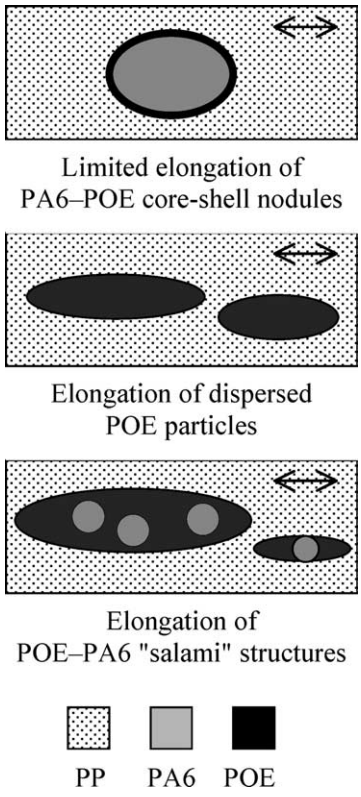

Fig. 9. Schematic presentation of different deformation and damage mechanisms.

'explodes' by nucleation and growth of an internal crack. This process releases significant amount of stored energy and reorganizes the stress field in the matrix with higher deviatoric stress component. This is the reason why cavitation is often observed in the POE phase of the BD15 and BD16 blends. According to configurations, voids are formed either in the isolated POE particles, in the POE interphase constituting the shell of the PA6–POE nodules, and in the POE phase of the complex 'salami' structures. Of course, when analyzing the micrographs, one took care in distinguishing the cavitation itself from the subsequent distortion induced by large deformation.

Apart the qualitative aspects of deformation and cavitation processes developed above, it is now important to interpret the quantitative importance of dilatation vs. the conservative deformation contribution. Fig. 2 shows that, on the overall, the $\varepsilon_v/\varepsilon_{33}$ ratio varies from 0.5 to 0.1 for our materials. Volume strain is high for neat PP and small for neat PA6. As for the PP/PA6/POE blends, they exhibit lower and lower volume strain as the total alloying content increases (except BD13 that is slightly over neat PP). This evolution is somewhat unexpectedly since, we could have envisaged, in a simplistic approach, that the activation of additional cavitation mechanisms in the blends (decohesion and cavitation) should have increased more and more the overall dilatation. Since experiments prove that this point of view is not true, the problem should be reconsidered on

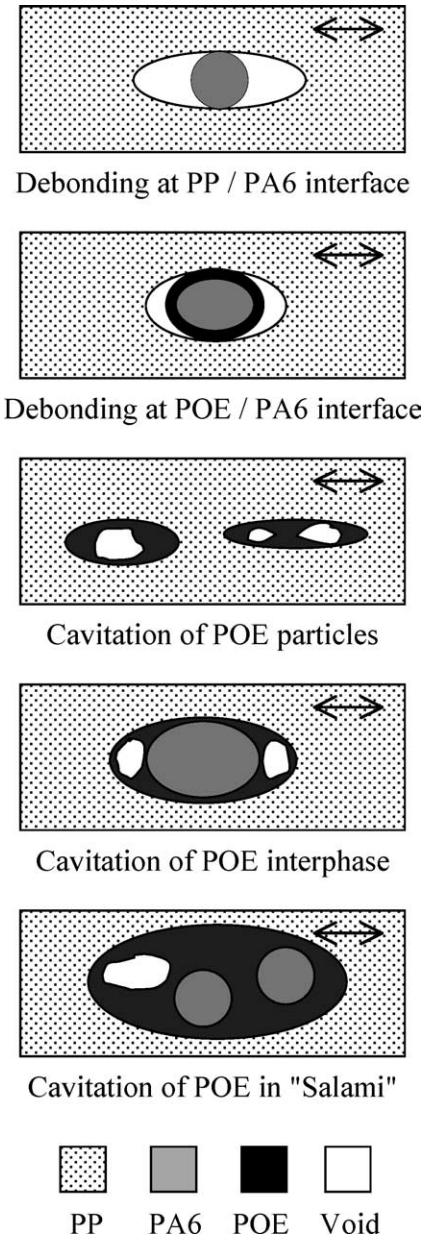

Fig. 10. Schematic presentation of different cavitation mechanisms.

more correct bases. A recent paper [23] have treated this question in the case of viscoelastic materials and led to the conclusion that the influence of cavitation on the overall response of the material depends to many factors like applied strain rate, particle-size distribution and relaxation time of matrix. Obviously developing a model valid for large strain plasticity would be much more complex and is not in the scope of this experimental paper. Consequently, we will just analyze here some arguments that may explain the observed facts.

The first point concerns the intrinsic properties of the materials constituting the blends. It is evident that, for the blends under consideration, we have mixed PP that suffers very high cavitation with increasing amounts of PA6 that deforms plastically with particularly low volume strain (Fig. 2). Although the PA6 phase does not support the same amount of strain in the blends than the PP matrix (PA6 particles shown little deformation in the micrographs), it is presumable that the lower tendency to cavitation of the blend is partly controlled by the more isochoric nature of the PA6 component.

The role of the POE phase is more complex. As many elastomers, it undergoes extensive cavitation when it is hydrostatically loaded within the interphase layers and the isolated nodules. However, it is often seen in the micrograph (especially after stress triaxiality has been releases by void nucleation) that POE is capable to undergo considerable stretching without further damage. The net effect could thus be to reduce volume strain.

Last but not least it should be envisaged that the nucleation of voids could have a positive effect on the plastic regime of the PP matrix itself. It has been shown before by many authors (and recently by van Melick et al. [24] using Finite Element calculation) that shear plasticity in a solid containing a random array of nanometric voids is considerably facilitated with respect to the same material in its compact form. Shear bands form between pairs of neighboring voids whose distance vector is inclined at nearly 45° on the tensile axis. As such, a diffuse network of percolating shear bands forms in the matrix causing easy plasticity. The ‘ligament’ model of Wu [25] is presented with slightly different words but is globally based on the same arguments. It is probable that plasticity enhancement due to the presence of voids is also relevant to our blends, where cavitation is early and finely dispersed. Unfortunately, the microscopic techniques used in this work do not make visible the shear plasticity mechanisms per se and are not capable to provide information on whether the above model is correct or not. It could be worthwhile to apply the atomic force microscopy technique to our samples in investigating this question more finely.

The experimental facts shown in this paper and the deformation scheme presented above are in line with a model previously proposed by Lazzeri et al. [26,27] to explain the interparticle distance effect on the basis of the stabilization effect of dilatational band propagation exerted by stretched rubber particles. Although dilatational bands were not formally identified in our specimens after deformation, the toughening effect of POE particles is definitely important in the PP/PA6/POE blends under investigation here.

Not only the above arguments help understanding the physics of deformation in the blends under consideration, but they can be utilized to guide the optimization of technical grades. As we showed it previously [5], increasing the (PA6+POE) content of the blend is highly favorable for mechanical engineering since, the resistance to impact (notched Izod impact strength) is increased by a factor of 5 by passing from BD13 to BD16, while the elastic modulus and yield stress are decreased by 20% only. Since, many

modifications are available in the preparation process, the qualitative model proposed above to explain microstructural and mechanical features constitutes a valuable to increase furthermore the performances of the blends.

5. Conclusions

For neat PP and PP/PA6/POE blends under tension, the microscopic study in this paper reveals the mechanisms that control the volume dilatation which was measured and presented in the previous paper of this series. Volume strain is particularly large for neat PP. It results from interlamellar crazes nucleated by crystal fragmentation and propagated along the radial direction in the spherulites. Under large strain, the cracks are turned towards the loading direction, forming large parallel 'empty channels'. The combinative use of SEM and TEM, as well as staining and etching techniques is necessary to obtain reliable characterization of polymer blends microstructures.

Both SEM and TEM show that debonding and cavitation represent the two factors to contribute to the volume increase of the blends studied. Interfacial debonding is preferentially observed at the poles of PA6 particles when the POE interphase is thin, that is in blends with low alloying content (BD13 and BD14). The interfacial arc-cracks are transformed into voids, and later into longitudinal cracks as plastic strain is increased. The cavitation occurs both at POE interphase around PA6 particles and in isolated POE particles. As to cavitation in isolated POE particles, it does not propagate out of these particles, so that the volume expansion generated is small.

As the alloying content is increased, it is observed that: (i) interfacial debonding of PA6 particle decreases, (ii) POE cavitation increases, (iii) elongation of dispersed POE particles increases and, (iv) plasticity of the PP matrix is enhanced. These evolutions explain why volume strain decreases, leading to a considerable increase of impact strength.

Acknowledgements

This work is supported by the National Natural Science Foundation of China under grant of 10272005, by the Excellent Young Teachers Program of MOE, People's Republic of China and by an advanced research program (PRA) between France and People's Republic of China. The authors are indebted to Mr Patrick Coupard, member of the Arkema laboratory, for performing the specimen characterization by transmission electron microscopy.

References

[1] Wu S. Polym Int 1992;29:229–47.
[2] Zebarjad SM, Bagheri R, Seyed Reihani SM, Lazzeri A. J Appl Polym Sci 2003;90:3767–79.
[3] Fond C, Lobbrecht A, Schirrer R. Int J Fract 1996;77:141–59.
[4] Bucknall CB, Heather PS, Lazzeri A. J Mater Sci 1989;16:2255–61.
[5] Bai SL, Wang GT, Hiver JM, G'Sell C. Polymer 2004;45:3063–71.
[6] G'Sell C, Bai SL, Hiver JM. Polymer 2004;45:5785–92.
[7] Wong SC, Mai YW. Polymer 1999;4:1553–66.
[8] Wong SC, Mai YW. Polymer 2000;41:5471–83.
[9] Gonzáles-Montiel A, Keskkula H, Paul DR. Polymer 1995;36:4587–603.
[10] Gonzáles-Montiel A, Keskkula H, Paul DR. Polymer 1995;36:4605–20.
[11] Gonzáles-Montiel A, Keskkula H, Paul DR. Polymer 1995;36:4621–37.
[12] G'Sell C, Hiver JM, Dahoun A. Int J Solids Struct 2002;39:3857–72.
[13] Olley RH, Hodge AM, Basset DC. J Polym Sci, Polym Phys Ed 1979;17:627.
[14] Vitali R, Montani E. Polymer 1980;21:1220–2.
[15] Trent JS, Scheinbeim JI, Couchman PR. Macromolecules 1983;16:589–98.
[16] Lazzeri A, Thio YS, Cohen RE. J Appl Polym Sci 2004;91:925–35.
[17] Aboulfaraj M, Ulrich B, Dahoun A, G'Sell C. Polymer 1993;34:4817–25.
[18] Aboulfaraj M, G'Sell C, Ulrich B, Dahoun A. Polymer 1995;36:731–42.
[19] Coulon G, Castelein G, G'Sell C. Polymer 1998;40:95–110.
[20] Lazzeri A, Bucknall CB. Polymer 1995;36:2895–902.
[21] Henning S, Adhikari R, Michler GH, Balta Calleja FJ, Karger-Kocsis. J Macromol Symp 2004;214:157–71.
[22] G'Sell C, Dahoun A, Favier V, Hiver JM, Philippe MJ, Canova GR. Polym Eng Sci 1997;37:1702–11.
[23] Chen JK, Huang ZP, Mai YW. Acta Mater 2003;51:3375–84.
[24] van Melick HGH, Govaert LE, Meijer HEH. Polymer 2003;44:457–65.
[25] Wu S. Polymer 1985;26:1855–63.
[26] Lazzeri A. Proceedings of the 10th international conference on deformation, yield and fracture of polymers, Cambridge, UK. London: The Inst. of Materials; 1997. p. 442–5.
[27] Zebarjad SM, Bagheri R, Seyed Reihani SM, Lazzeri A. J Appl Polym Sci 2003;90:3767–79.